



TECHNICAL ARTICLE

Reproducibility of Cell Structure and Mechanical Properties of Al-Si-Mg/SiC_p Composite Foams in Relation to the Foaming Temperature

Ravi K. Nadella, Jagan R. Ginuga, Sampath K. Pati, and Amol A. Gokhale

Submitted: 10 July 2022 / Revised: 12 September 2022 / Accepted: 24 October 2022 / Published online: 14 November 2022

A359 aluminum alloy composite containing 20 vol. % silicon carbide particles was remelted, and 100-mm diameter foam ingots were prepared using 0.75 wt. % of titanium hydride (TiH₂). Three identical experiments each were carried out at two foaming temperatures (640 and 660 °C) to check the reproducibility of the cell structure and foam properties. Foams made at 640 °C were reproducible in terms of foam expansion, cell size and cell size variation along the ingot height. The property scatter, evaluated in terms of relative standard deviation, is similar for density and modulus of the foam. For compressive plastic strength, the scatter is double than for density. The density and mechanical properties are reproducible within these scatters. Foams prepared at 660 °C, on the other hand, suffered from liquid foam collapse during solidification and hence couldn't be qualified for detailed study of reproducibility. The collapse resulted in distortion of the foam ingot and elongated cell structures in other parts. However, the cell size and mechanical properties in the un-distorted region are comparable with those foamed at 640 °C. Overall, good quality cell structure and consistent mechanical properties could be obtained in foams processed at 640 °C.

Keywords Al-Si foam, composite foam, compression, modulus

1. Introduction

Closed-cell metal foams have ultra-low densities (0.2 to 0.8 g/cm³) and are good energy absorbers at low-transmitted stresses (Ref 1). Further, they have a combination of properties such as good fire resistance (in comparison with polymer foams), lower thermal conductivity, better mechanical damping as compared to the parent material. Aluminum-calcium foams are well known in closed-cell metal foams category (Ref 2).

Aluminum-based closed-cell foams can also be produced with aluminum alloy composites containing ceramic particles where the particles act as foam stabilizers (Ref 3, 4). Since the cell wall material influences the foam properties, high strength of the composite based on a heat treatable matrix alloy is beneficial. There may also be structural changes within the cell wall as observed for melt-processed aluminum foam where the grains in cell walls are smaller than for a pore-free material (Ref. 5). Increasing SiC content is beneficial in improving high temperature compressive properties in Al-alloy/SiC foams (Ref. 6). Further, these composite foams can be utilized in thin wall

tubes to improve the crashworthiness (Ref. 7). While efforts were made to foam various aluminum alloy-ceramic particle composites by melt processing (Ref 8), including Al-Si/SiC composites (Ref 4, 9, 10), the reproducibility of the properties was hardly reported in the literature. For the same density, Kennedy observed that the scatter in properties is in the range of 2 to 5% of the mean values (Ref 11).

This matter is of concern with reference to the commercial manufacturing of aluminum foams. Therefore, the reproducibility of the cell structure and the properties has been evaluated as a function of foaming temperature, which is a crucial process parameter.

A melt-based batch process was used for making aluminum alloy-SiC_p composite foams. In this work, a pre-made composite was re-melted and foamed using an external foaming agent. The reproducibility of these foams is presented in terms of cell size, density, elastic modulus, and compression properties.

2. Experimental Methods

2.1 Foaming Procedure

An A359 cast alloy (chemical composition in wt. %: Al-9.4Si-0.55 Mg-0.15Fe) composite containing 20 vol. % SiC_p was used in this work. The measured median size of SiC particles is 6.3 μm. Microstructure of as-received cast composite (Fig. 1) showed angular morphology of SiC_p with the matrix containing eutectic Si. The liquidus temperature of this composite as measured by differential scanning calorimetry is 586 ± 1 °C (Fig. 2). This is slightly lower than the liquidus temperature of 592 °C reported for the same composite (Ref 9).

Ravi K. Nadella, Jagan R. Ginuga, and Sampath K. Pati, Novel Manufacturing Technologies Group, Defense Metallurgical Research Laboratory, Kanchanbagh Post Office, Hyderabad 500 058, India; and Amol A. Gokhale, Department of Mechanical Engineering, Indian Institute of Technology Bombay, Powai, Mumbai 400 076, India. Contact e-mail: ravikumar.dmlr@gov.in.

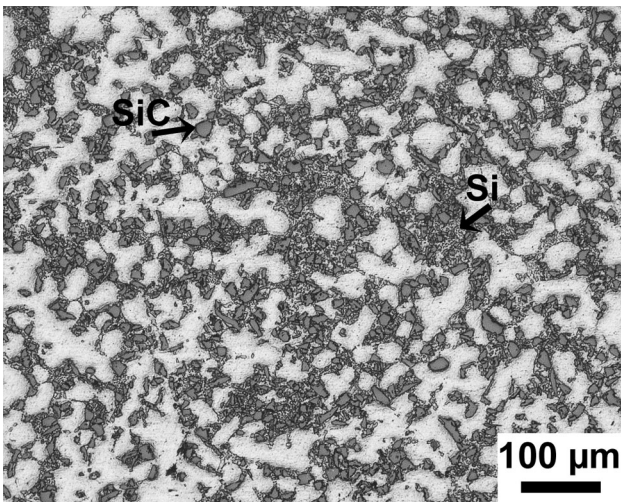


Fig. 1 SiC particle morphology and eutectic Si in the as-received cast A359 composite

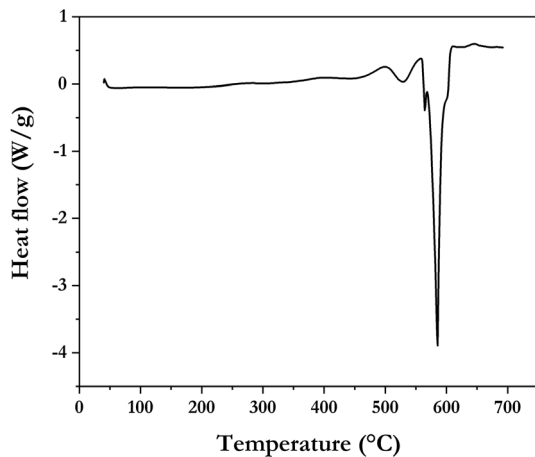


Fig. 2 DSC plot for A359-20% SiC composite

Titanium hydride (TiH_2) powder was used as the foaming agent. In melt-processed foams, the particle size of TiH_2 powder is important for better mixing and homogeneous distribution in the liquid melt. Fine particles tend to coagulate and don't mix well in the melt, while too coarse particles dissociate slowly increasing the total foaming time which is likely to produce a wider cell size distribution in the foam. In the present case, TiH_2 with a particle size (d_{50}) of $11 \mu\text{m}$ is used.

Foaming experiments were carried out with 0.75 wt. % of TiH_2 at 1.35 kg melt size to make 100-mm diameter cylindrical foam ingots. A schematic diagram along with a flow chart is given in Fig. 3 to indicate the steps involved in foam synthesis by melt-processing. Cut pieces of aluminum composite ingot were melted in a clay graphite crucible at 700°C . The oxides were skimmed and the melt was mechanically stirred slowly to keep the SiC particles in suspension. This was necessary to avoid undue enhancement in viscosity which could potentially obstruct uniform mixing of the foaming agent in the melt subsequently (Ref 12). After cooling the melt to the desired foaming temperature, the melt was again stirred to unsettle SiC_p and TiH_2 powder was mixed under continued stirring to initiate

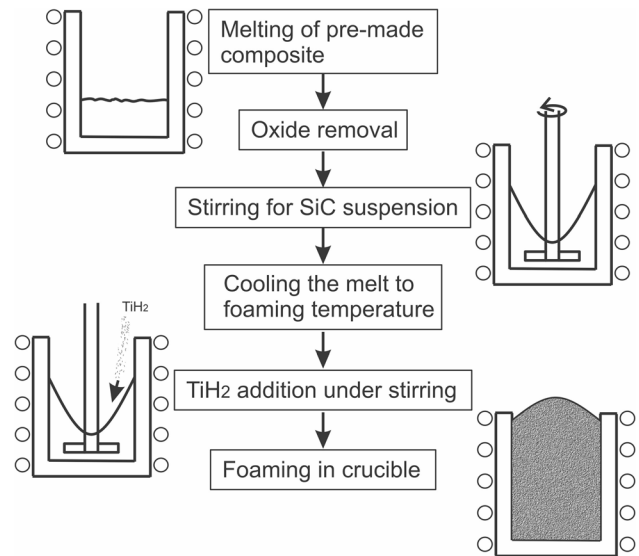


Fig. 3 Flow chart and schematic diagram showing the processing steps in A359-SiC composite foam making

the foaming. Once the foam stopped rising, as observed visually, the crucible was taken out and was cooled under forced-air. Two foaming temperatures (640°C and 660°C) were chosen with differential superheats and, at each temperature, three identical trials were carried out. These six ingots were designated as DU-1A, DU-1B, DU-1C (prepared at 640°C) and DU-2A, DU-2B, DU-2C (prepared at 660°C).

2.2 Structural Characterization and Property Evaluation

At each experiment, the liquid foam height, and the solidified foam height were measured. These heights were normalized by the initial melt height to arrive at total expansion, and net expansion, respectively. Cylindrical foam ingots were sectioned longitudinally by wire electric discharge machining (EDM). Cell sizes were measured on optically scanned cross sections at 20-mm interval along the foam height which is also the foaming direction. At least 80 individual cell measurements were done on $20 \text{ mm} \times 100 \text{ mm}$ area along superimposed random lines perpendicular to the foaming direction. Metallographic samples were polished with standard procedures followed for aluminum composites.

Samples for dynamic Young's modulus measurements ($75 \times 30 \times 10 \text{ mm}$) were extracted by wire EDM with sample thickness (10 mm) parallel to the foaming direction (Fig. 4). The sample length (75 mm) was kept symmetric across the ingot centerline. The ratio of sample length to the minimum dimension was kept above 5 as per ASTM E-1876. Room temperature Young's modulus (E^*) was determined by impulse excitation of vibration using resonant frequency damping analyzer (RFDA). During this test, the $75 \times 30 \text{ mm}$ rectangle was supported at nodal points and excited using an automatic impulse exciter. The excitation signal was captured using a microphone and, after subsequent analysis using Fast Fourier Transform in RFDA software, the flexural resonant frequency was extracted. From this frequency, E^* was determined.

Compression test specimens of $20 \times 20 \times 25 \text{ mm}$ were cut by wire EDM from the sectioned foam ingot on either side of the centerline (Fig. 4). The shape and dimensions of the sample were as per ISO 13314 – 'Compression testing of cellular

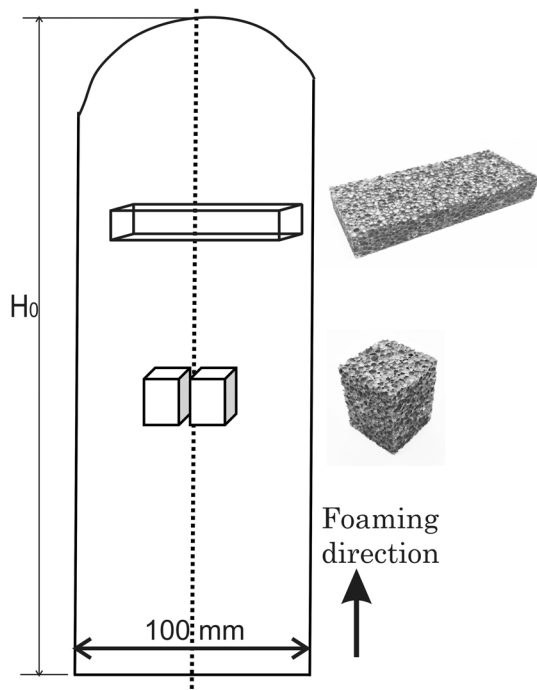


Fig. 4 Schematic diagram illustrating the extraction of test samples from the longitudinally sectioned foam ingot along with actual foam samples

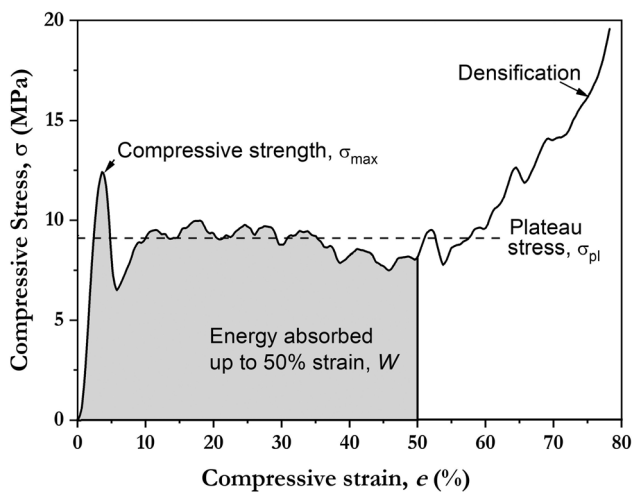


Fig. 5 Typical compression curve of an A359-SiC_p foam sample illustrating extracted parameters (relative density = 0.154)

materials' (Ref 13). Considering the cell sizes (≈ 1.4 mm) in our foams, sample dimensions were selected so that each dimension is at least 10 times the average cell size (Ref 13). The sample length (25 mm) was kept aligned with the foaming direction (Fig. 4). Compression test was carried out on a servo-hydraulic machine (Instron Model No. 5500R). The foam sample was compressed at a constant cross-head speed of 5 mm/min (an initial strain rate of $3.3 \times 10^{-3} \text{ s}^{-1}$) between

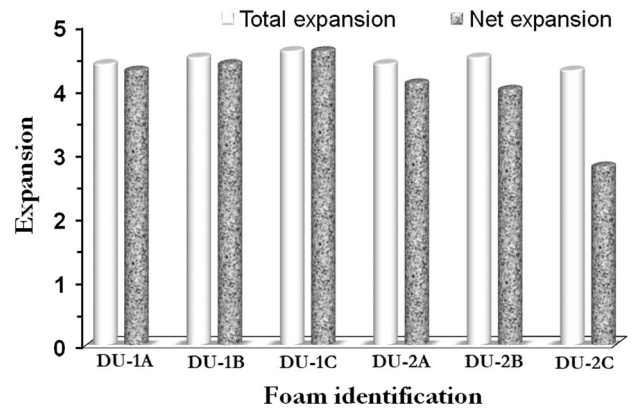


Fig. 6 Total and net expansion data for foam ingots prepared at 640 °C (DU-1A, DU-1B, DU-1C), and at 660 °C (DU-2A, DU-2B, DU-2C)

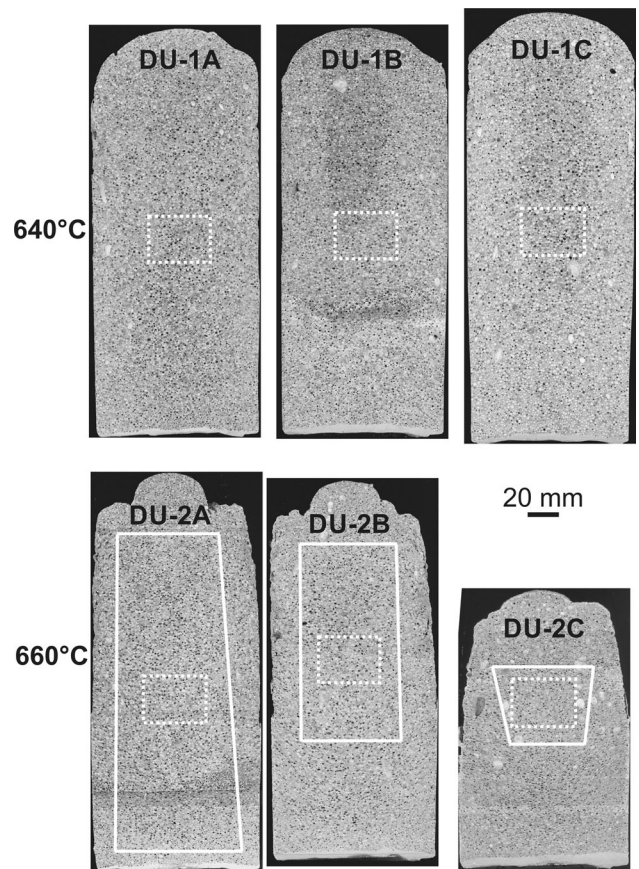


Fig. 7 Longitudinal mid-sections of foam ingots prepared at 640 , and 660 °C. Areas within the broken lines are magnified in Fig. 8. For ingots prepared at 660 °C, an estimated undistorted region is marked with a solid line

steel loading platens along the length using graphite flakes as a lubricant. The recorded load–displacement data were converted to stress–strain ($\sigma - \epsilon$) curves.

In the $\sigma - \epsilon$ plot (Fig. 5), stress corresponding to the first local maximum (first maximum compressive strength; Ref 13)

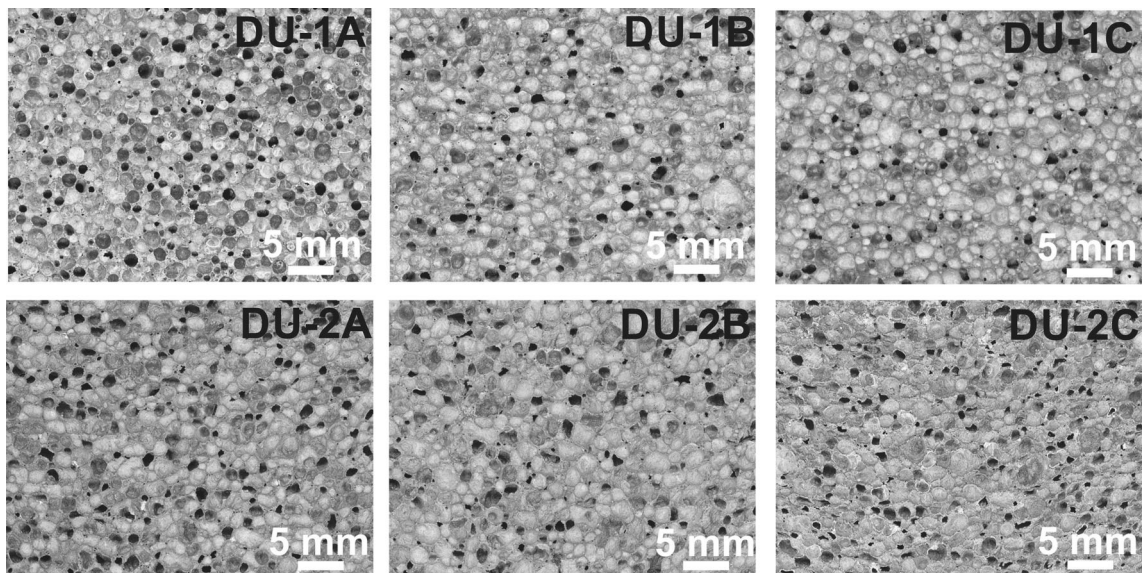


Fig. 8 Magnified images of foams (marked with broken lines in Fig. 7)

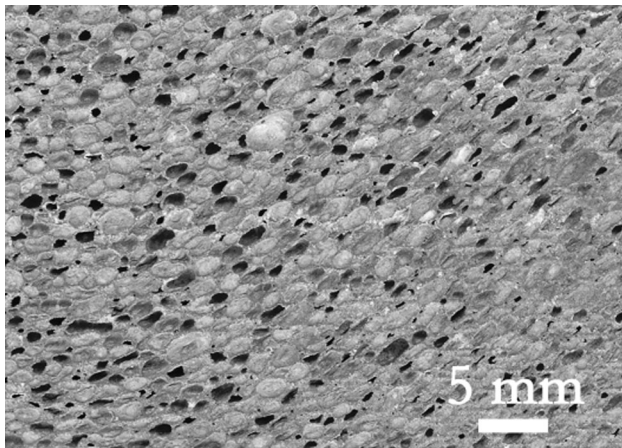


Fig. 9 Distorted region showing deformed/ elongated cells in foams prepared at 660 °C

is termed as ‘compressive strength’ (designated as σ_{\max}) in the present work. The plateau stress (σ_{pl}) was computed as the average of the stresses between 20 and 40% compressive strain intervals. The energy absorbed (W) and the energy absorption efficiency (W_e) were calculated up to 50% strain by equations:

$$W = \frac{1}{100} \int_0^{50} \sigma de \quad (\text{Eq 1})$$

$$W_e = \frac{W}{\sigma_o \times 50} \times 10^4 \quad (\text{Eq 2})$$

where σ_o is the maximum stress between 0 and 50% strain.

Foam density (ρ^*) was obtained from the measured weights and physical dimensions of individual test samples, from which the relative density (ρ^*/ρ_s) was calculated. The density of the cell wall material (ρ_s) was computed as 2.79 g/cm³ from the rule of mixtures for A359-20% SiC composite.

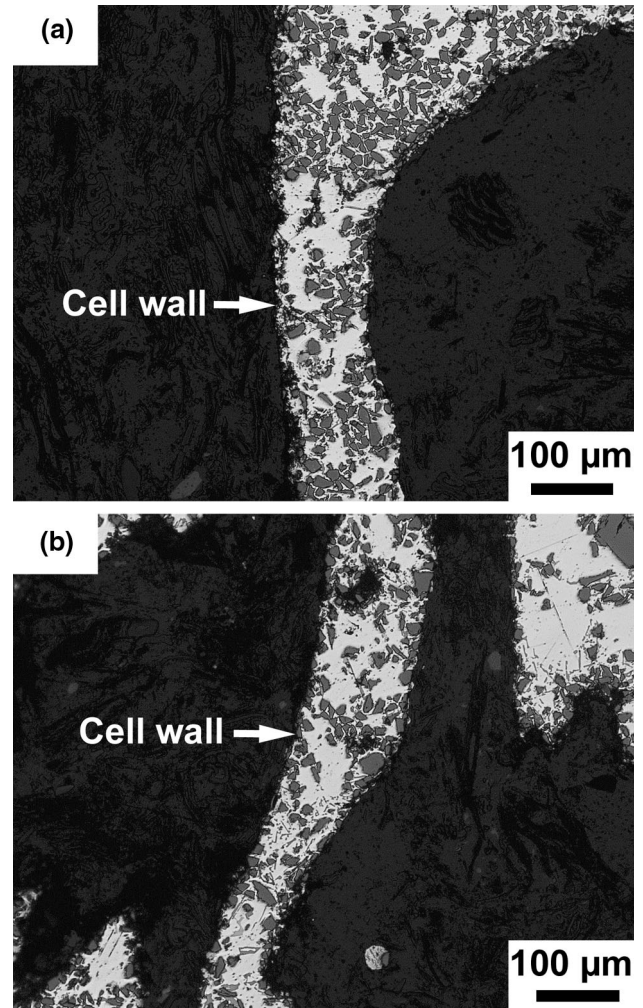


Fig. 10 Cell wall structures in A359-20% SiC composites foamed at 640 °C (a), and 660 °C (b)

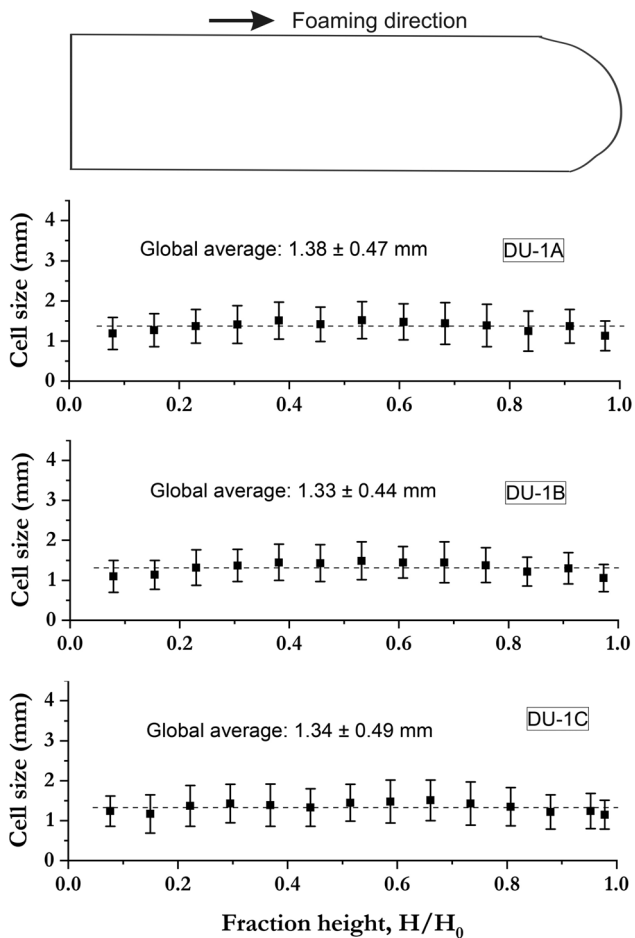


Fig. 11 Individual cell size (mean \pm standard deviation) measurements along the height for three foams prepared at 640 °C. The global average (average cell size obtained for the whole ingot) along with the standard deviation is given for each foam ingot. The horizontal line in each plot indicates the global average

3. Results and Discussion

3.1 Temperature Effect on Foam Stability, and Cell Size

The total and net expansion data for foams prepared at 640 and 660 °C is given in Fig. 6. For each experiment, foam collapse is the difference between total and net expansions. Foamability (the ability of the melt to reach large expansions) is quantified by the total expansion. Foam stability (the ability of the foam to remain structurally intact until complete solidification), on the other hand, is assessed by the net expansion. At a given foaming temperature, the total expansions are identical for the three experiments indicating consistent foamability. From the moment TiH_2 addition is initiated, it dissociates, releasing hydrogen and forming gas bubbles, leading to melt expansion. This expansion involves gas diffusion to bubbles, their growth and likely coalescence due to rapid impingement among the rising bubbles (Ref 14, 15). The SiC particles present in the melt not only decrease the surface tension (Ref 8), aiding bubble formation, but also increase the melt viscosity, which slows the film drainage and downward liquid flow in the liquid foam (Ref 16).

Also, despite 20 °C variation, the foamability changed little between two foaming temperatures, mainly due to constant

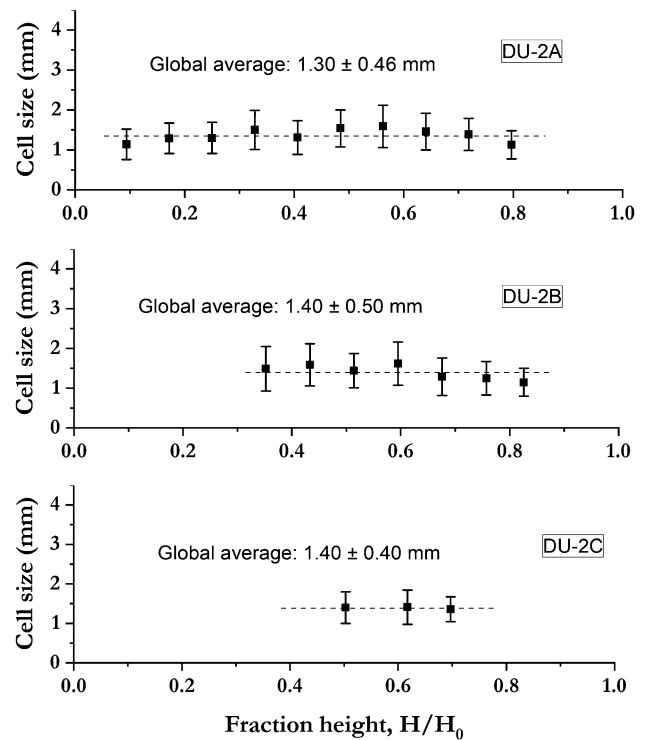
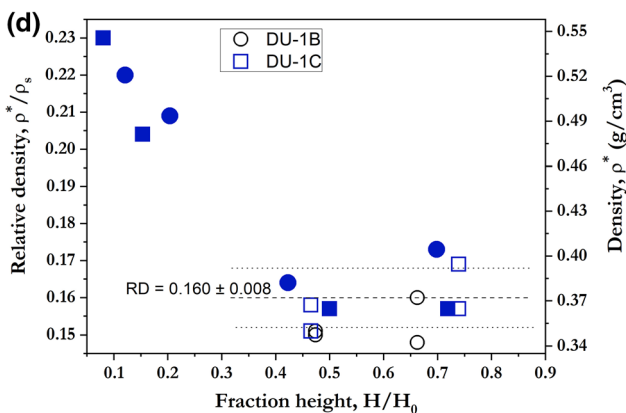
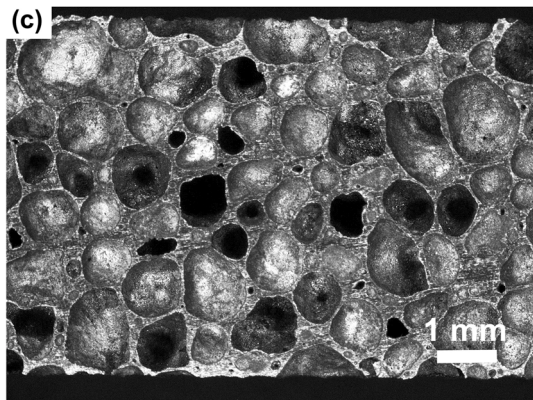
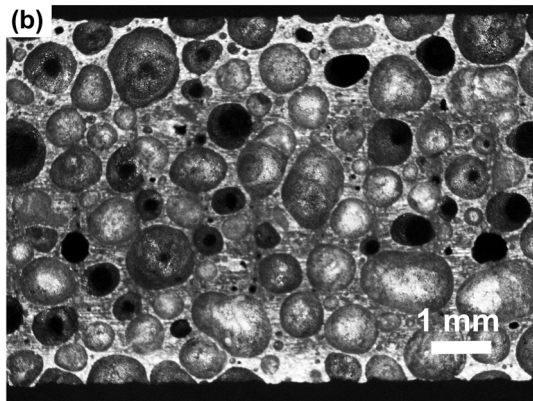
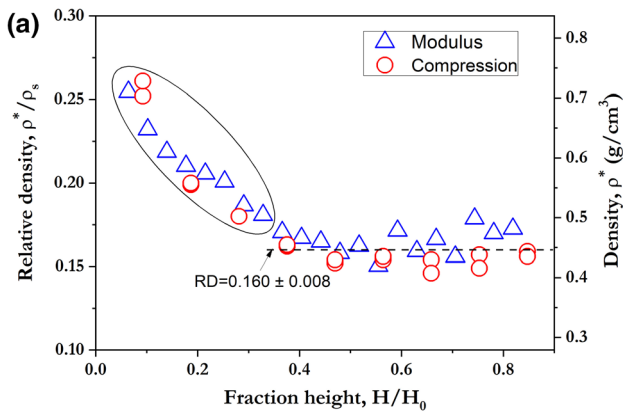


Fig. 12 Cell size (mean \pm standard deviation) variation along the height for foams prepared at 660 °C. Cell sizes were measured only in the undistorted regions (see Fig. 7). The horizontal line in each plot indicates the global average

TiH_2 addition. Higher temperatures, however, increase the TiH_2 dissociation rate (Ref 17).

During cooling, the foam either retained the total expansion (Fig. 6) showing good stability (negligible collapse at 640 °C) or exhibited varying collapse indicating instability (as observed at 660 °C). The macrostructures of foam ingots (Fig. 7) show the absence of cracks extending to several cells. The magnified pictures presented in Fig. 8 further confirm individual cells without cell wall ruptures. The collapse at 660 °C manifested as distorted regions with elongated cells (Fig. 9) within the ingot. The absence of very large cells with significant liquid drainage points out that the liquid foam might have collapsed under its own weight. In comparison with 640 °C-foams, the decay at 660 °C is certainly associated with longer cooling times from the foaming temperature to the liquidus temperature. Further, the liquid foam may also be structurally weak with reduction in strength of the liquid film network ($\approx 15\%$ of the foam volume considering the relative density is around 0.15) at a higher temperature. One can argue that the ‘resistance to collapse’ would be dependent on the temperature of the melt and a temperature difference of 20 °C (in the present case 640 °C versus 660 °C) may be significant.

Microstructures showed that the SiC particles are randomly distributed within the cell walls (including at the cell surfaces) and Plateau areas at both the foaming temperatures (Fig. 10). Unlike other studies on this system (Ref 18), particles’ preference to solid/gas interface is not observed. The presence of the SiC particles at the cell surface can be explained based on the fact that the particles are partially wetted by the melt, which can result in stable bubble-particle configurations (Ref 16) and increased surface viscosity (Ref 19). Removal of oxides during



◀ **Fig. 13** Relative density (RD) data and structures of 640 °C-foams: (a) RD as varied with DU-1A foam height. The local average RD, determined after excluding the circled data points, is shown by a broken line. Foam structures at 20 mm (b), and 140 mm (c) heights exhibiting varying cell wall thicknesses. (d) RD data from compression (open symbols), and modulus (filled symbols) samples extracted from DU-1B & DU-1C ingots at selected heights. The data beyond 90 mm is compared to the local mean \pm standard deviation (shown as broken line and dotted lines, respectively) obtained for DU-1A

composite remelting also has a destabilizing effect, specifically at 660 °C, as was shown for A359-SiC composite foaming (Ref 8). Presence of eutectic Si is evident (Fig. 10b) similar to the as-received composite structure (Fig. 1).

The cell size measurements were carried out for all ingots along the height. For 660 °C- foams, a region of undistorted cells was estimated by visual observation (bordered with a solid line; Fig. 7). Figure 11 and 12 show the cell size data in the form of individual values of mean and its variations of standard deviation (SD) at each location for foams of 640 °C and 660 °C, respectively. For convenience, the foam height is represented as a fraction height along the X-axis (H_0 is the foam height; Fig. 4). For each foam ingot, average cell size for the whole ingot (henceforth termed as global average) is given.

At 640 °C, it is evident that for the three ingots, the global averages are within the individual cell size variations meaning uniform cell size along the foam height. For DU-1A, the SD is around 35% of the global average cell size (relative standard deviation, RSD). It is also clear that the global average cell sizes (≈ 1.4 mm) and their RSDs are identical ($\approx 35\%$) showing reproducibility in cell structures along the entire foam ingot. For 660 °C, the cell size didn't vary significantly both within the ingots and in between three ingots as shown by the average cell size and SD data (Fig. 12).

3.2 Density and Mechanical Properties

In view of the collapse and associated distortion of foams prepared at 660 °C, detailed study was not possible. This section mainly describes the properties of 640 °C- foams and present their variation and extent of property scatter among three experiments. For this, detailed density measurements were done for one foam ingot (DU-1A) with test samples extracted at various foam heights (Fig. 4). For the other two ingots (DU-1B & DU-1C), the samples were extracted at selected heights.

The data (Fig. 13a) shows that the relative density (RD) decreased up to 90 mm from the ingot bottom, beyond which it changed little. The maximum RD is 0.26 ($\rho^* = 0.73$ g/cm³) at the ingot bottom which decreased to around 0.16 RD ($\rho^* = 0.45$ g/cm³). The density gradient within the bottom portion of the foam may largely be attributed to gravity-induced liquid drainage through the network of struts (Plateau borders) toward the foam bottom as was observed in melt-processed aluminum foams (Ref 20). Liquid drainage resulted in thicker cell walls in the bottom portion of the foam ingot as shown in

Table 1 Experimental properties obtained for an ingot prepared at 640 °C

| | Relative density | | E-Modulus (GPa) | | Compressive strength (MPa) | | Plateau stress (MPa) | | Energy absorbed (MJ/m ³) | | Energy absorption efficiency (%) | |
|-----------------|------------------|--------------------|-----------------|-------|----------------------------|-------|----------------------|-------|--------------------------------------|-------|----------------------------------|-------|
| | Global* | Local [#] | Global | Local | Global | Local | Global | Local | Global | Local | Global | Local |
| | 1 | 2 | 3 | 4 | 5 | 6 | 7 | 8 | 9 | 10 | 11 | 12 |
| Mean | 0.179 | 0.160 | 6.17 | 5.26 | 14.7 | 12.1 | 11.9 | 9.51 | 5.80 | 4.55 | 77.6 | 75.4 |
| SD [§] | 0.031 | 0.008 | 1.38 | 0.33 | 4.5 | 1.2 | 4.1 | 0.92 | 2.09 | 0.43 | 4.6 | 2.6 |
| Column No | 1 | 2 | 3 | 4 | 5 | 6 | 7 | 8 | 9 | 10 | 11 | 12 |

*Average calculated from the whole data [#]Average calculated after excluding the data up to 90 mm foam height (0.3 fraction height)
[§]Standard deviation

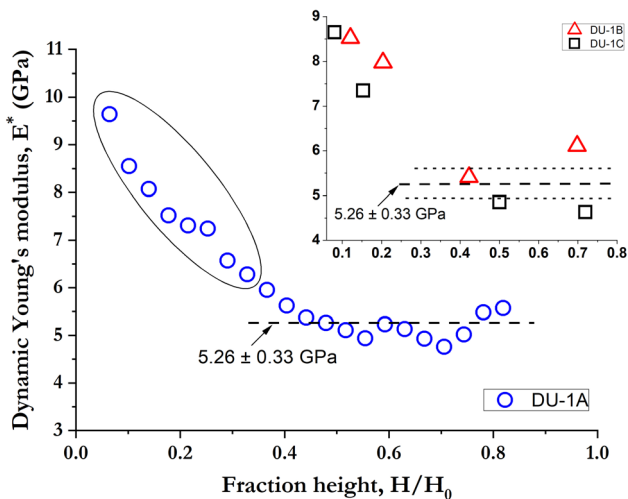


Fig. 14 Dynamic Young's modulus data (E^*) data for 640 °C-foams. The variation of E^* with foam height is presented for DU-1A ingot. Local average E^* , determined after excluding the circled data points, is shown by a broken line. In the inset graph, the moduli for samples extracted from DU-1B & DU-1C at selected locations are compared to the local mean \pm standard deviation (shown as broken and dotted lines)

Fig. 13(b) and (c) which compares the average cell wall thickness of 1.83 mm (at 20 mm height) with 0.93 mm (at 140 mm height). For equivalent cell size (Fig. 11), thicker cell walls mean higher density. Overall, the presence of 20 vol. % particles coupled with forced-air cooling of liquid foams helped in limiting the drainage as shown by the thin layers of un-foamed metal at the bottom of the foam ingots (Fig. 7).

As given in Table 1, the global average RD is 0.179 ± 0.031 with an RSD of 17%. The marginally changed density above 90 mm height (0.3 fraction height) is clear from the local average RD i.e., 0.160 ± 0.008 , with an RSD of 5%, obtained after ignoring the data below 90 mm (circled points in Fig. 13a). Density data for samples extracted from other ingots (DU-1B and DU-1C) beyond 0.3 fraction height are within this deviation (Fig. 13d). Also, increased density is observed below 0.3 fractional heights in line with trends in Fig. 13a.

In line with density data (Fig. 13a), E^* decreased up to 90 mm height beyond which it didn't vary appreciably with increasing height (Fig. 14). With reference to its global average (Table 1), the RSD is 22% which is slightly higher than that for density (17%). The local average modulus obtained after ignoring the data below 90 mm height (circled points in

Fig. 14) is 5.26 ± 0.33 GPa i.e., RSD of 6%. This scatter is in line with the density scatter (5%) within the same height (Fig. 13a). Modulus data obtained from samples of other foam ingots (DU-1B & DU-1C) are almost matching (inset graph in Fig. 14) with the data obtained for DU-1A.

The local average modulus was predicted using the local average RD (0.160 ± 0.008 ; Fig. 13a; column 2 in Table 1) by Ashby – Gibson (A-G) equations (Ref 21) for metal foams

$$\frac{E^*}{E_s} = \left(\varphi \frac{\rho^*}{\rho_s} \right)^2 + (1 - \varphi) \frac{\rho^*}{\rho_s} \quad (\text{Eq 3})$$

The value of E_s , the dynamic Young's modulus of the cell wall material, is measured as 104.7 GPa for A359-20% SiC composite. The term φ is the fraction of material at cell struts (nodes). With a value of 0.8 for 0.13 RD Al-SiC foam (Ref 22), φ was assumed as 0.75 considering the RD of 0.160 in the present case. The A-G model value of E^* is 5.70 ± 0.21 GPa which is in good agreement with the experimental value of 5.26 ± 0.33 GPa (column 4 in Table 1).

Data (Fig. 15) shows that the compression properties (σ_{\max} , σ_{pl} , and W) exhibited similar trends as the modulus and changed marginally beyond 90 mm foam height. This trend is in expected line with the density variation (Fig. 13a). Global average values of σ_{\max} , σ_{pl} , and W , are given in Table 1 with RSD being 31%, 35%, and 36%, respectively. This is almost double the global density variation of 17%. The local average properties obtained after ignoring the data below 90 mm height (Fig. 15) are 12.1 ± 1.2 MPa (σ_{\max}), 9.51 ± 0.92 MPa (σ_{pl}), and 4.55 ± 0.43 MJ/m³ (W). The RSD values are 9.9%, 9.7%, and 9.5%, respectively, which are again double the density variation (i.e., 5%) shown for local average RD.

It is seen that the scatter in properties is higher in the upper regions of the foam. This could be due to the fact that these regions experience the maximum depletion of melt due to drainage which thins the cell walls producing very dry foams. Such cell structures are vulnerable to coarsening and, hence, development of locally large cells which reduce the plastic strength, since it refers to the initiation of plastic deformation in the weakest region of the foam.

The changes in W_c are not as drastic as the other compressive properties. This property too decreased up to 90 mm, and remained constant (75.4 ± 2.6) beyond 90 mm height, with the global average of 77.6 ± 4.6 (Fig. 15d). The RSD is around 6% for the global average and 3.4% for the local average.

Compression properties obtained from selected samples of other foam ingots (DU-1B & DU-1C) are within the average values obtained for DU-1A (inset graphs in Fig. 15).

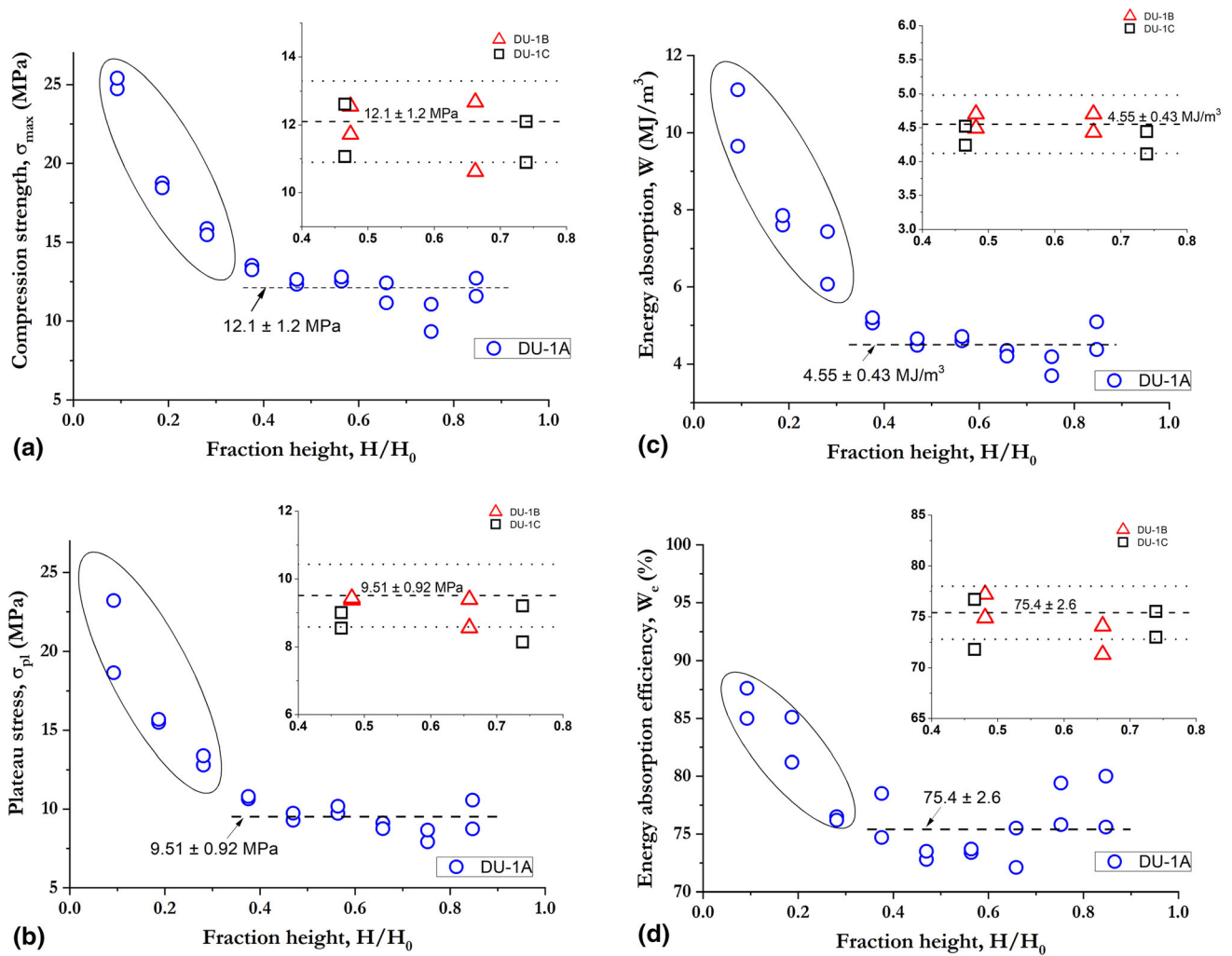


Fig. 15 Compression properties for 640 °C-foams. For each property, local average (shown by a broken line) was calculated after excluding the circled data points. In the inset graphs, property data obtained for samples extracted from DU-1B & DU-1C ingots at selected locations is compared to the local mean \pm standard deviation (shown as broken line and dotted lines, respectively) obtained for DU-1A. (a) Compression strength, σ_{\max} ; (b) Plateau stress, σ_{pl} ; (c) Energy absorbed, W ; and (d) Energy absorption efficiency, W_e

Table 2 Summary of density and mechanical properties of 660 °C-foams

| Sample ID | Fraction height | Relative density | Dynamic Young's modulus, GPa | Compressive strength, MPa | Plateau stress, MPa | Energy absorbed, MJ/m ³ | Energy absorption efficiency, % |
|-----------|-----------------------------|------------------|------------------------------|---------------------------|---------------------|------------------------------------|---------------------------------|
| DU-2A | 0.35 | 0.177 | 5.63 | — | — | — | — |
| | 0.59 | 0.154 | — | 11.1 | 8.8 | 4.34 | 78.3 |
| DU-2B | 0.59 | 0.146 | — | 10.7 | 7.8 | 3.86 | 72.1 |
| | 0.34 | 0.182 | 5.72 | — | — | — | — |
| | 0.51 | 0.158 | — | 11.7 | 9.1 | 4.46 | 76.3 |
| DU-2C | 0.51 | 0.144 | — | 10.1 | 7.9 | 3.80 | 75.5 |
| | —Data couldn't be obtained— | | | | | | |

The collapse strength equivalent to plateau stress is predicted using the average density below 90 mm height (0.160 ± 0.008 ; Fig. 13a) in the A-G equation (Ref 21).

$$\frac{\sigma_{pl}^*}{\sigma_s} = 0.3 \left(\varphi \frac{\rho^*}{\rho_s} \right)^{3/2} + (1 - \varphi) \frac{\rho^*}{\rho_s} \quad (\text{Eq 4})$$

In the above equation, the yield strength of cell wall material, σ_s , is taken as 205 MPa which is measured for A359-20% SiC composite. With φ assumed as 0.75, the A-G model value of σ_{pl}^* (10.8 ± 0.4 MPa) is close to the experimental σ_{pl} of 9.51 ± 0.92 MPa (column 8 in Table 1).

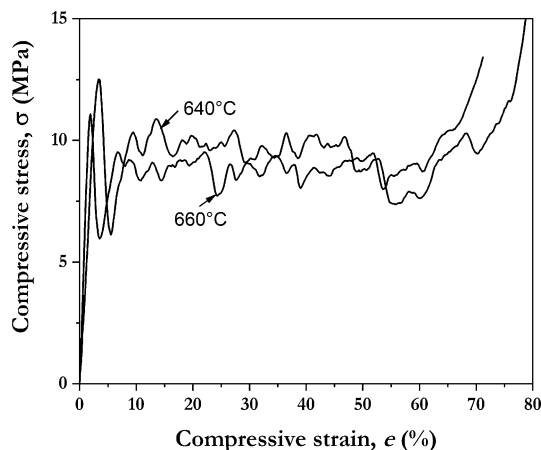


Fig. 16 Compression stress–strain curves at 0.154 RD for foams obtained at two temperatures

Excellent foam quality and near absence of defects gave rise to a good correlation of experimental values with A–G model predictions for both plateau stress and elastic modulus.

As stated earlier, a part of the foam prepared at 660 °C was distorted due to collapse and was not used for further analysis. However, there was sufficient volume of foam which was not distorted and which possessed sound cellular structure. This was used to extract a few samples for compression tests and elastic modulus measurements from selected heights within the foam. The summary of density and property data are given in Table 2. It is clear that for the given density levels in 660 °C-foams, the modulus and compression properties are comparable to the data obtained for 640 °C-foams. Further, the nature of compressive deformation is similar as seen from the curves obtained at 640 and 660 °C (Fig. 16).

4. Summary

1. Foams prepared at 640 °C showed reproducible expansion, cell size at given height and cell size variation with foam height.
2. In 640 °C-foams, the scatter in compression properties, evaluated in terms of relative standard deviation, is double the scatter obtained in density. The scatter in the elastic modulus is equivalent to that of density.
3. The A359-20% foams properties are close to the Ashby - Gibson model predictions.
4. Foams made at 660 °C exhibited liquid foam collapse before complete solidification. In regions without signs of foam collapse, the properties are on par with foams prepared at 640 °C.

Acknowledgments

This work is supported by Defense Research and Development Organization. The authors are grateful to Dr Phani Mylavarapu for carrying out modulus measurements.

References

1. J. Baumeister, J. Banhart and M. Weber, Aluminum Foams for Transport Industry, *Mater. Des.*, 1997, **18**, p 217–220
2. T. Miyoshi, M. Itoh, S. Akiyama and A. Kitahara, ALPORAS Aluminum Foam: Production Process, Properties, and Applications, *Adv. Eng. Mater.*, 2000, **2**, p 179–183
3. O. Prakash, H. Sang and J.D. Embury, Structure and Properties of Al-SiC Foam, *Mater. Sci. Eng. A.*, 1995, **199**(2), p 195–203
4. M.C. Gui, D.B. Wang, J.J. Wu, G.J. Yuan and C.G. Li, Deformation and Damping Behaviors of Foamed Al-Si-SiC_p Composite, *Mater. Sci. Eng., A*, 2000, **286**, p 282–288
5. L. Hu, Y. Li, X. Zhou and G. Yuan, Characterization of As-cast Microstructure of Aluminum Foams by Melt Foaming Method, *Mater. Lett.*, 2022, **308**, p 131112
6. A. Dehnavi, GR. Ebrahimi and M. Golestanipour, Effect of SiC Particles on Hot Deformation Behavior of Closed-cell Al/SiC_p Composite Foams, *J. Braz. Soc. Mech. Sci. Eng.*, 2020, **42**, p 554
7. M. Rogala, J. Gajewski and K. Gawdzińska, Crashworthiness Analysis of Thin-walled Aluminum Columns Filled With Aluminum–silicon Carbide Composite Foam, *Compos. Struct.*, 2022, **299**, 116102
8. N. Babcsán, D. Leitlmeir and H.P. Degischer, Foamability of Particle Reinforced Aluminum Melt, *Materialwiss. Werkstofftech.*, 2003, **34**, p 22–29
9. N. Babcsán, F. Garcia Moreno and J. Banhart, Metal Foams—High temperature Colloids Part II: In Situ Analysis of Metal Foams, *Colloids Surf A*, 2007, **309**(1–3), p 254–263
10. Y. Luo, Yu. Sirong, W. Li, J. Liu and M. Wei, Compressive Behavior of SiC_p/AlSi₁₀Mg Composite Foams, *J. Alloys Compd.*, 2008, **460**, p 294–298
11. A.R. Kennedy, Aspects of the Reproducibility of Mechanical Properties in Al Based Foams, *J. Mater. Sci.*, 2004, **39**, p 3085–3088
12. R. Nadella, JR. Ginuga, S. Pati, and A. Gokhale, Foaming and Compressive Properties of A359/SiC_p Metal Matrix Composites, *Mater. Sci. Forum*, 2018, **941**, p 1920–1926
13. Mechanical Testing of Metals-Ductility testing -Compression test for porous and cellular metals, ISO 13314, International organization for standardization, 2011
14. C. Körner, M. Arnold, M. Theis and R.F. Singer, 2002, The Physics of Foaming: Structure Formation and Stability, *Handbook of Cellular Metals: Production, Processing, and Applications*, H. P. Degischer, and B. Kriszt, eds., Wiley-VCH Verlag GmbH, Weinheim, Germany
15. S.N. Sahu, A. Gokhale and A. Mehra, Bubble Size Distribution in Foaming of Liquid Aluminum and the Role of Coarsening and Coalescence, *Adv. Eng. Mater.*, 2017, **19**, p 1600745
16. S.W. Ip, Y. Wang and J.M. Toguri, Aluminum Foam Stabilization by Solid Particles, *Can. Metall. Q.*, 1999, **27**, p 81–92
17. C.C. Yang and H. Nakae, Foaming Characteristics Control During Production of Aluminum Alloy Foam, *J. Alloys Compd.*, 2000, **313**, p 188–191
18. L.D. Kenny, Mechanical Properties of Particle Stabilized Aluminum Foam, *Mater. Sci. Forum*, 1996, **217–222**, p 1883–1890
19. V. Gergely, H.P. Degischer and T.E. Clyne, Recycling of MMCs and Production of Metallic Foams, *Compr. Compos Mater*, 2000, **3**, p 797–820
20. Z.K. Cao, B. Li, G.C. Yao and Y. Wang, Fabrication of Aluminum Foam Stabilized by Copper-coated Carbon Fibers, *Mater Sci Eng A*, 2008, **486**(1–2), p 350–356
21. L.J. Gibson and M.F. Ashby, *Cellular solids: structure and properties*, Cambridge University Press, Cambridge, United Kingdom, 1997
22. M. Guden and S.J. Yüksel, SiC-particulate Aluminum Composite Foams Produced from Powder Compacts: Foaming and Compression Behavior, *J. Mater. Sci.*, 2006, **41**, p 4075–4084

Publisher's Note Springer Nature remains neutral with regard to jurisdictional claims in published maps and institutional affiliations.

Springer Nature or its licensor (e.g. a society or other partner) holds exclusive rights to this article under a publishing agreement with the author(s) or other rightsholder(s); author self-archiving of the accepted manuscript version of this article is solely governed by the terms of such publishing agreement and applicable law.